Liesegang Banding for Controlled Size and Growth of Zeolitic-Imidazolate Frameworks

Rita Zakhia Douaihy, Mazen Al-Ghoul, and Mohamad Hmadeh**

Here, the formation of periodic precipitation (Liesegang bands) from hybrid (organic–inorganic) components is reported, namely ZIF-8, ZIF-67, and their mixed metal derivatives. The spacing and width laws that characterize the Liesegang system are determined and the resulting pattern is exploited to crystal engineer various sizes and doping of the ZIF material. Several key parameters that govern the crystallization process of ZIF-8 are investigated in each band and the growth of the particles in each band is found to follow an Ostwald ripening mechanism.

Zeolitic imidazolate frameworks (ZIFs) represent a distinctive subclass of metal–organic frameworks (MOFs)[1] that consists of M-IM-M units where M refers to the metal cations (e.g., Zn (II), Co (II)), and IM refers to the Imidazolate linkers (e.g., 2 methyl-Imidazole, benzimidazole). Their importance is due to their porosity,[2] high crystallinity,[3] and chemical[3,4] and thermal stability.[3–5] They are used in various applications including separation and gas storage,[6,7] catalysis,[5] encapsulation of small molecules[8] and drug delivery.[9] Therefore, the control of the size and morphology of their crystals is considered an essential endeavor.[10] Particularly, ZIF-8[3,4] is one of the most studied ZIF material that is characterized by a robust porous structure[3] and has been synthesized using various techniques.,[3,11] Interestingly, when Zn(II) cations are partially or totally substituted by cobalt within the same ZIF-8 topology,[10c,12] the resulting heterometallic framework exhibited enhanced gas separation and photocatalytic properties.[13] However, the direct synthesis of these heterometallic ZIFs is a challenging task due to the possible separation into a physical mixture of ZIF-8 and ZIF-67, in addition to the difficulty of controlling the cobalt-doping percentage within the same framework.

A new method for the synthesis of MOF-199[14] and ZIF-8[15] via a reaction–diffusion framework (RDF)[16] was recently developed by our group. RDF is a method that involves continuous precipitation reactions triggered by diffusing a concentrated solution of one coprecipitate (outer electrolyte) into a tube containing a gel medium with the other coprecipitate (inner electrolyte).[17] The gist of this method is based on establishing a propagating supersaturation wave whose extent decreases as it moves down the tube. Since crystal nucleation and growth highly depend on supersaturation, this setup translates into a gradient in crystal sizes extending over space: small crystals are incepted early on where nucleation dominates, and larger crystals grow farther where growth governs the crystallization of the product.[18] In specific mineral systems, the nonlinear coupling of precipitation reactions with crystal nucleation and growth leads to the formation of a pattern consisting of a series of alternative precipitate bands separated by precipitate-free zones,[19] which is known as the Liesegang banding phenomenon[16,20] (Scheme S1, Supporting Information). This banding phenomenon is governed by various scaling laws that portray the detailed macroscopic features of the emerging pattern. The spacing law[16,21] characterizes the increasing distance between consecutive bands and is illustrated by the spacing coefficient p extracted from the slope of the linear plot of x_{n+1} versus x_n in the equation

$$x_{n+1}/x_n = 1 + p \tag{1}$$

where x_n denote the location of the n^{th} band. The dependence of the spacing coefficient on the inner (b_0) and outer (a_0) concentrations is given by the Matalon–Packter law according to the following equation[22]

$$p = F(b_0) + G(b_0)/a_0 \tag{2}$$

The width law,[16,23] which characterizes the width w_n of the n^{th} band located at x_n is written as

$$w_n = x_n^{\alpha} \tag{3}$$

where the width exponent can be extracted from the log–log plot of Equation (3). The control of the spacing parameter p and exponent allows us to design well-separated bands with adjustable thickness, which can be exploited in the control of particle size, dispersion, and ease of extraction. While the Liesegang phenomenon has only been observed in a large variety of sparingly soluble inorganic salts,[24] there has been so far no reports of Liesegang patterns in hybrid or other materials. Herein, we describe the first Liesegang system made of ZIF-8, ZIF-67, and their solid solution crystals. This system is characterized by the scaling laws described above. Furthermore, we show how to

R. Zakhia Douaihy, Prof. M. Al-Ghoul, Prof. M. Hmadeh
Department of Chemistry
American University of Beirut
PO Box 11-0236, Riad El Solh, Beirut 1107-2020, Lebanon
E-mail: mazen.ghoul@aub.edu.lb; mohamad.hmadeh@aub.edu.lb
The ORCID identification number(s) for the author(s) of this article can be found under https://doi.org/10.1002/smll.201901605.

DOI: 10.1002/smll.201901605

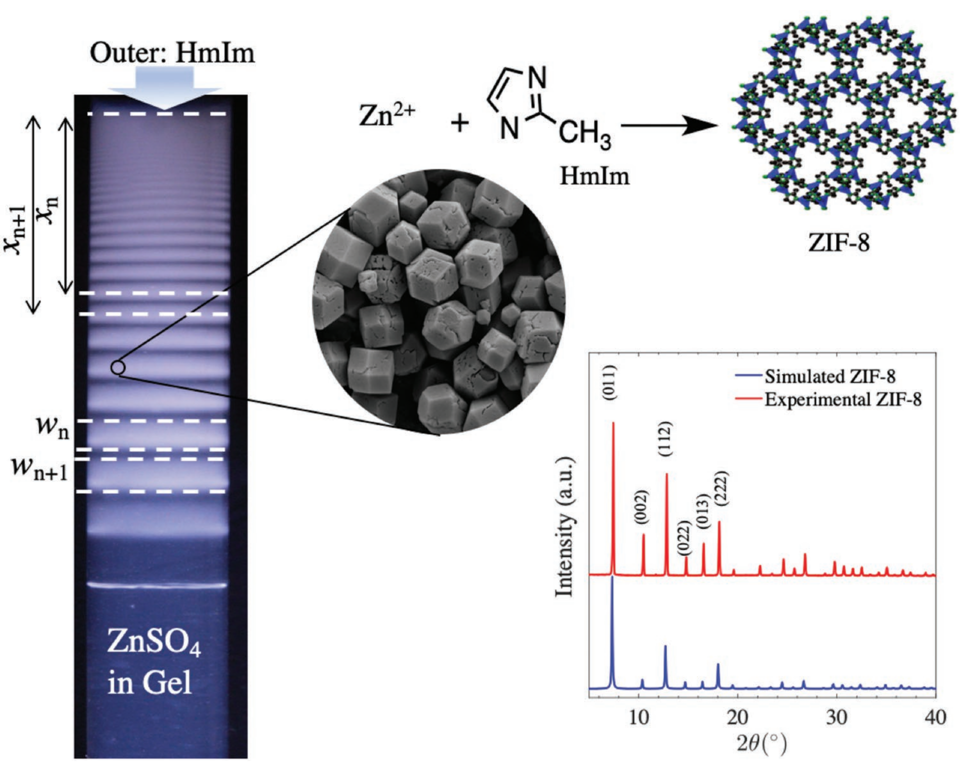

Figure 1. Synthesis of ZIF-8 crystals via the Liesegang banding in the reaction–diffusion framework (RDF). Polyhedral crystals, observed within different bands in the tube, are identified as ZIF-8 by comparing its PXRD pattern (red) with the simulated pattern of ZIF-8 (blue).

exploit the Liesegang pattern to engineer ZIF monodispersed single crystals with various sizes and doping compositions.

Liesegang bands of ZIF-8 particles are formed by using zinc sulfate (or cobalt sulfate in the case of ZIF-67) as the inner electrolyte and the organic linker 2-methylimidazole (HmIm) as the outer solution. A hot solution of zinc sulfate is dissolved in a hydrogel (1% agar) with an equal volume of *N*,*N*-dimethylformamide (DMF). After gelation in a tube, an aqueous solution of 2-methylimidazole is poured on its top (see the Experimental Section in the Supporting Information for more details). In the case of the doping experiments, mixtures of zinc and cobalt sulfate with various compositions are used as inner electrolytes. The diffusion of the HmIm solution into the gel matrix leads to the formation of a white precipitate (purple in the case of cobalt) as shown in **Figure 1**. After 3 days of propagation, the precipitation region of the tube is divided into equidistant consecutive zones of 0.5 cm thickness. They are thereafter extracted and washed several times in hot DMF and dichloromethane (DCM) to dissolve the gel and remove unreacted species, then dried in a vacuum oven at 100 °C. The dried powder is then subjected to powder X-ray diffraction (PXRD) analysis for structural identification. The obtained PXRD pattern is assigned to ZIF-8 diffraction pattern, with all its main peaks (Figure 1). No additional peaks are observed, which reveals the purity of the sample.

After we established the identity of the crystals, the spacing and width laws that characterize the macroscopic features of the Liesegang pattern are investigated. The measurements of the band position x_n and the band width w_n are carried out using digital photography and Adobe Photoshop and plotted versus the band number n (Figure S1, Supporting Information). The spacing coefficient p and the width exponent α are then computed as shown in **Table 1**. For this system, p ranges between 0.114 and 0.230. These positive values indicate an increasing spacing between the bands thus defining a direct spacing precipitation system.[25] Moreover, α varies between 1.10 and 1.60 following the same trend stated by Droz et al.[23] By combining the scaling considerations with the conservation law of the number of particles obtained is close to 1. Furthermore, the Matalon–Packter law for this system (Equation (2)), reveals that F and G are increasing functions of b_0 in contrast to other different systems where F and G are decreasing functions of the inner concentrations.[22]

The morphology of the collected particles from the extracted zones is then investigated using scanning electron microscopy (SEM) after being coated with a layer of gold. Starting at the gel-outer solution interface of zone 1, spherical ZIF-8 particles are obtained at the first minute of growth followed by a transition to polyhedral particles after 5 min (Figure S2, Supporting

Table 1. Spacing coefficient p and width exponent α as a function of the inner [Zn^{2+}] and outer [HmIm].

	Inner concentration [$\times 10^{-3}$ M]			Outer concentration [M]		
	5.0	10	20	0.5	1.0	1.5
p	0.114(6)	0.128(7)	0.153(4)	0.230(2)	0.222(4)	0.203(5)
α	1.10(6)	1.13(9)	1.50(9)	1.60(8)	1.44(6)	1.30(7)

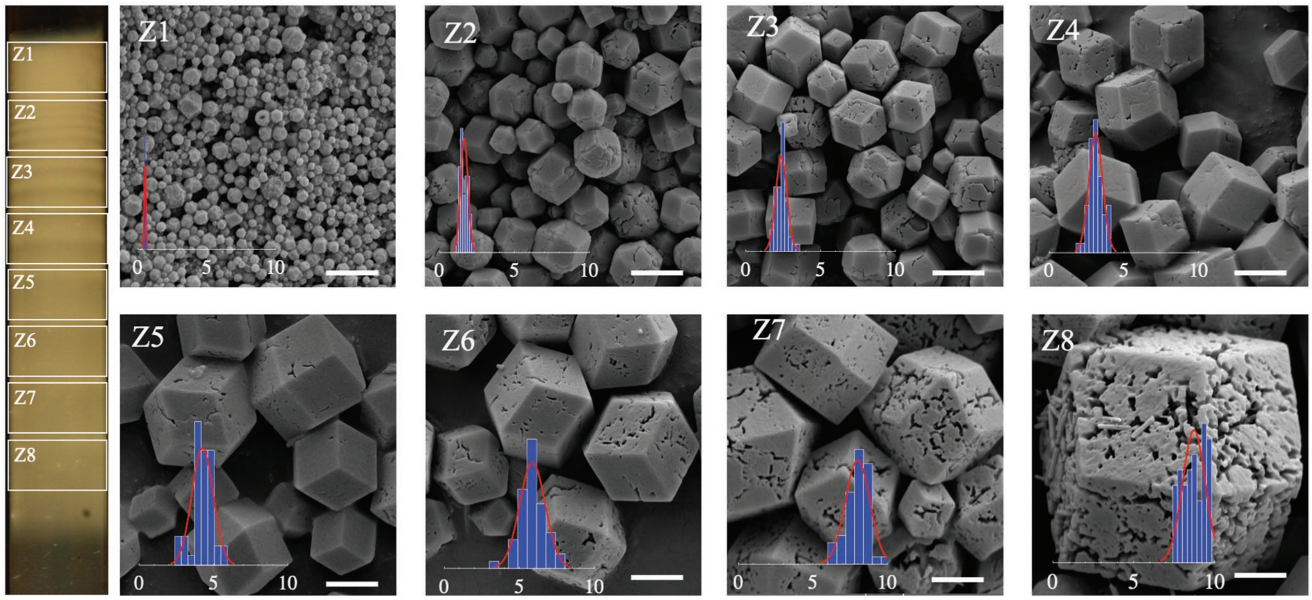

Figure 2. Scanning electron microscopy images of ZIF-8 obtained from six consecutive zones (0.5 cm thickness) with $[Zn^{2+}] = 20 \times 10^{-3}$ M and [HmIm] = 1.0 M and 1% gel at 25 °C. The insets represent the particle size distribution in each zone (µm). The scale bar is 2 µm.

Information). Going down the tube through different zones, the SEM images show sharp edged polyhedral crystals with increasing particle size. Moreover, although the particle size distribution (insets in **Figure 2**) increases as we move into lower zones, it is still relatively narrow. This trend is a characteristic of RDF, whereby smaller particles are obtained at the interface where nucleation dominates (highest supersaturation) and bigger particles are formed away where the rate of crystal growth surpasses the rate of nucleation (Figure 2). This quasi-linear trend in particle size is in agreement with previous work on inorganic systems.[18b] Particularly, we observe an increase in the spongy character[26] of the ZIF polyhedra as we go far from the interface regardless of the outer concentrations, the agar percentage and the temperature (Figure 2 Z6 and Figures S3–S6, Supporting Information). Furthermore, the collected crystals from various zones are subjected to Brunauer–Emmett–Teller BET and thermogravimetric analysis (TGA). The N_2 adsorption isotherm of the activated sample is carried out and the BET surface area is calculated to be 1430 $m^2\ g^{-1}$ for our ZIF-8, which is in accordance with the reported values (Figure S7a, Supporting Information). Moreover, the thermal stability (up to 550 °C) is further confirmed by TGA (Figure S7b, Supporting Information). These analyses implicate that the RDF technique does not overall affect the structural and textural properties of the synthesized ZIF despite the observed macro porosity in later zones. More importantly, this synthesis approach is found to be scalable by simply using large reactor instead of a small tube and similar Liesegang banding is observed therein (Figure S8, Supporting Information).

The Liesegang banding is then exploited to engineer monodisperse ZIF crystals and perform controlled cobalt doping on them. For this aim, various experiments are carried out using different adjustable experimental parameters such as the concentration of the reactants, the temperature and the gel percentage. In all these cases, assorted trends are obtained, and we are able to obtain crystal sizes ranging from ≈100 nm to ≈7 µm across the different zones within the same tube. We also notice that the dispersity of the particle size extracted from all the zones is very small. At a fixed outer concentration [HmIm] = 1.0 M the size of the ZIF particles increases with the inner $[Zn^{2+}]$ and starts to differentiate appreciably after the third zone (**Figure 3**a). On the other hand, the trend is reversed for fixed inner $[Zn^{2+}] = 20 \times 10^{-3}$ M and increasing outer concentration [HmIm] (Figure 3b). The concentration of agar is also a major parameter in RDF. While the gel provides a convection-free environment of a better crystal growth process, it also restricts the final size that the crystals reach within its pores. In fact, a relatively high gel percentage leads to a decrease in the average gel pore size, an increase in the number of nucleation sites and a decrease in the rate of growth due to the augmentation of the number of defects.[27] This results in a decrease in the average particle size as clearly exhibited in Figure 3c. where smaller crystal sizes are consistently obtained at higher gel percentage. Additionally, the effect of temperature on the average particle size is investigated. The increase of the temperature is accompanied by an increase in the rates of nucleation and growth, thus leading to an increase in the particle size as shown in Figure 3d and Figures S3–S6 (Supporting Information). It is also noticeable that although the speed of the reaction–diffusion process has increased with temperature, leading to larger distances of propagation (location of the last zone in Figure 3d) as well as to larger widths of the individual Liesegang bands, the dispersity of the particle size among the zones is not affected and remains markedly small. The growth of the particles in each band is found to follow an Ostwald ripening[28] as evidenced from the value of the exponent γ of the fit (Figure S9,

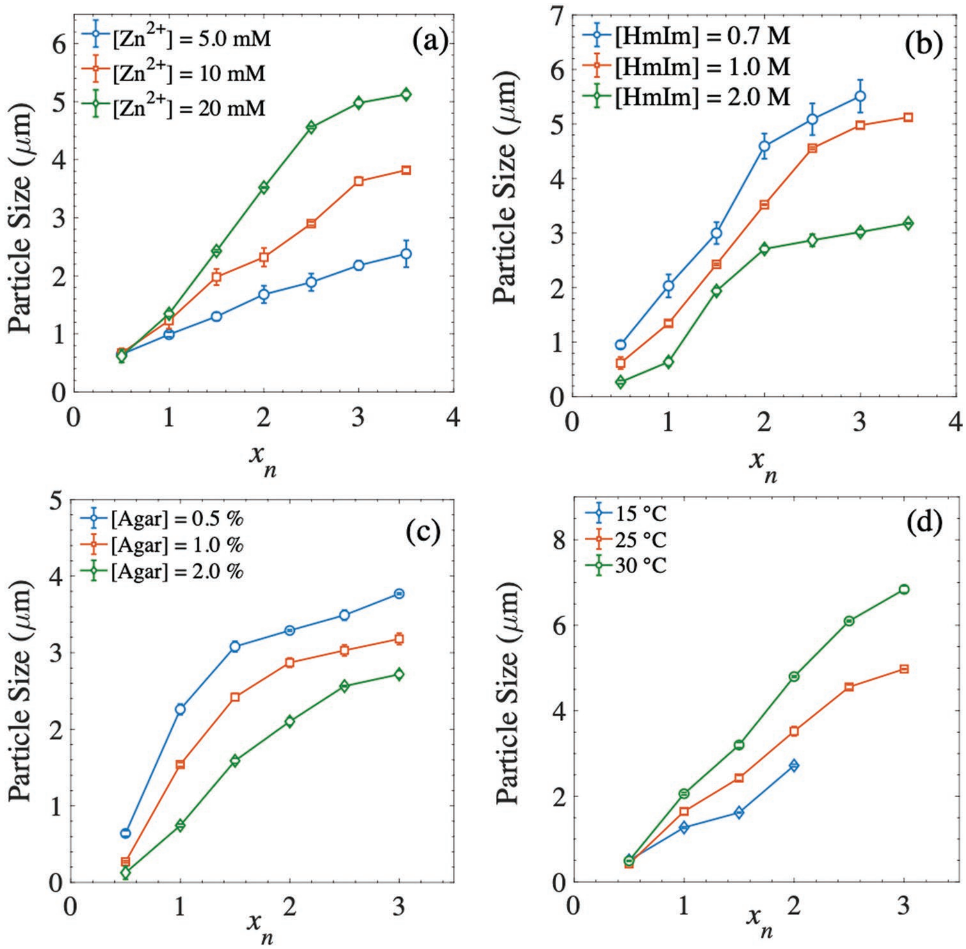

Figure 3. Particle size of ZIF-8 particles as a function of the zone position x_n at a) different inner concentrations ([HmIm] = 1.0 M, 1% gel), b) different outer concentrations ($[Zn^{2+}] = 20 \times 10^{-3}$ M, 1% gel), c) different agar percentages ($[Zn^{2+}] = 20 \times 10^{-3}$ M, [HmIm] = 2.0 M), and d) different temperatures ($[Zn^{2+}] = 20 \times 10^{-3}$ M, [HmIm] = 1.5 M, 1% gel). The error bars represent the standard error on the mean with a number of particles $N = 100$.

Supporting Information) of the average size of the particles (D_t) in zone 1 as a function of time (t)

$$D_t = \left[D_0^{1/\gamma} + k\,(t - t_0) \right]^{\gamma} \tag{4}$$

where γ is 0.30 that is close to 1/3, which favors an Ostwald ripening mechanism.

Mixed metal Zn-Co-ZIFs can be also synthesized following the same procedure by using different initial concentrations of cobalt and zinc salts in the outer solution. Purple Liesegang bands are observed until zinc is completely replaced by cobalt when a continuous (not discrete) precipitation zone of ZIF-67 emerges. The average size of the doped crystals is the same as those in pure ZIF-8 under the same conditions. The final metal ion composition in five consecutive zones (**Figure 4**) is then determined using atomic absorption (see the Experimental Section in the Supporting Information for more details). At all ratios of initial concentrations ($R_0 = [Co]_0$:$[Zn]_0$), the incorporation of cobalt into the ZIF structure in all the five zones was efficient and determined to be slightly smaller than R_0 (Figure 4). Fascinatingly, the SEM images of the solid extracted from the leading Z5 region reveal a 2D nanosheet-like morphology whereas well-defined polyhedral particles are obtained in the preceding zones (Z1-Z3). The PXRD pattern of the nanosheets is attributed to ZIF-L. This type of polymorphic transformation from ZIF-L to ZIF-67 was recently reported.[29] Z4 in Figure 4 represents the phase transition region where the attachment of the nanosheets to form polyhedral structures is observed (Figure 4).

In conclusion, we report for the first time a hybrid organic–inorganic system, namely ZIF-8 that exhibit Liesegang bands. The macroscopic Liesegang laws that govern the emerging pattern are then exploited to crystal engineer ZIF-8, ZIF-67 and their mixed metal derivative in a controlled manner. Consequently, crystal sizes ranging from about 100 nm to a few microns can be obtained. Moreover, the composition of mixed metal ZIF can be also be tuned. We show that the crystals within the bands grow via Ostwald ripening. Such reaction–diffusion mechanism can thus be utilized to make various MOF and ZIF material with mixed metal and/or mixed linkers.

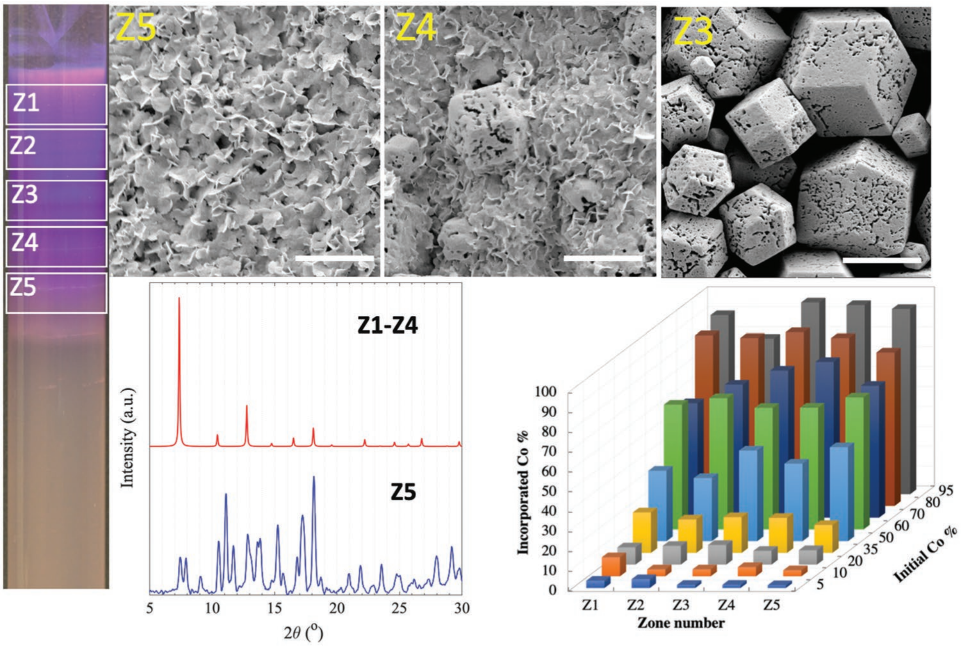

Figure 4. SEM images of different zones as labeled on the reaction tube. Sheets extracted from Z5 correspond to ZIF-L as indicated in the XRD pattern. The sheets transform to ZIF-67 crystals in Z3. Z4 corresponds to the transition region between the 2D and the 3D crystals. The doping of cobalt as a function of zone number and initial cobalt concentration is shown in the 3D bar graph.

Supporting Information

Supporting Information is available from the Wiley Online Library or from the author.

Acknowledgements

The authors acknowledge the funding provided by the American University of Beirut Research Board and the K. Shair Central Research Science Laboratory. The authors also thank Manal Ammar for her help in some of the experimental work.

Conflict of Interest

The authors declare no conflict of interest.

Keywords

controlled size, crystal growth, mixed metals, periodic precipitation, zeolitic imidazolate frameworks

Received: March 28, 2019
Revised: May 2, 2019
Published online: May 30, 2019

[1] a) H.-C. Zhou, J. R. Long, O. M. Yaghi, *Chem. Rev.* **2012**, *112*, 673; b) A. Phan, C. J. Doonan, F. J. Uribe-Romo, C. B. Knobler, M. O'keeffe, O. M. Yaghi, *Acc. Chem. Res.* **2010**, *43*, 58; c) M. Eddaoudi, D. F. Sava, J. F. Eubank, K. Adil, V. Guillerm, *Chem. Soc. Rev.* **2015**, *44*, 228; d) B. Chen, Z. Yang, Y. Zhu, Y. Xia, *J. Mater. Chem. A* **2014**, *2*, 16811.
[2] P. Gómez-Álvarez, S. Hamad, M. Haranczyk, A. R. Ruiz-Salvador, S. Calero, *Dalton Trans.* **2016**, *45*, 216.
[3] K. S. Park, Z. Ni, A. P. Côté, J. Y. Choi, R. Huang, F. J. Uribe-Romo, H. K. Chae, M. O'Keeffe, O. M. Yaghi, *Proc. Natl. Acad. Sci. USA* **2006**, *103*, 10186.
[4] S. R. Venna, M. A. Carreon, *J. Am. Chem. Soc.* **2010**, *132*, 76.
[5] U. P. Tran, K. K. Le, N. T. Phan, *ACS Catal.* **2011**, *1*, 120.
[6] H. Hayashi, A. P. Cote, H. Furukawa, M. O'Keeffe, O. M. Yaghi, *Nat. Mater.* **2007**, *6*, 501.
[7] R. Banerjee, A. Phan, B. Wang, C. Knobler, H. Furukawa, M. O'keeffe, O. M. Yaghi, *Science* **2008**, *319*, 939.
[8] H. Mieno, R. Kabe, N. Notsuka, M. D. Allendorf, C. Adachi, *Adv. Opt. Mater.* **2016**, *4*, 1015.
[9] C.-Y. Sun, C. Qin, X.-L. Wang, G.-S. Yang, K.-Z. Shao, Y.-Q. Lan, Z.-M. Su, P. Huang, C.-G. Wang, E.-B. Wang, *Dalton Trans.* **2012**, *41*, 6906.
[10] a) W. Sun, X. Zhai, L. Zhao, *Chem. Eng. J.* **2016**, *289*, 59; b) L. H. Wee, M. R. Lohe, N. Janssens, S. Kaskel, J. A. Martens, *J. Mater. Chem.* **2012**, *22*, 13742; c) G. Kaur, R. K. Rai, D. Tyagi, X. Yao, P.-Z. Li, X.-C. Yang, Y. Zhao, Q. Xu, S. K. Singh, *J. Mater. Chem. A* **2016**, *4*, 14932.
[11] a) Y.-R. Lee, M.-S. Jang, H.-Y. Cho, H.-J. Kwon, S. Kim, W.-S. Ahn, *Chem. Eng. J.* **2015**, *271*, 276; b) J.-H. Park, S.-H. Park, S.-H. Jhung, *J. Korean Chem. Soc.* **2009**, *53*, 553.
[12] a) J. K. Zaręba, M. Nyk, M. Samoć, *Cryst. Growth Des.* **2016**, *16*, 6419; b) X. Wang, X. Fan, H. Lin, H. Fu, T. Wang, J. Zheng, X. Li, *RSC Adv.* **2016**, *6*, 37965.
[13] a) C. Wang, F. Yang, L. Sheng, J. Yu, K. Yao, L. Zhang, Y. Pan, *Chem. Commun.* **2016**, *52*, 12578; b) P. Krokidas, M. Castier, S. Moncho, D. N. Sredojevic, E. N. Brothers, H. T. Kwon, H.-K. Jeong, J. S. Lee, I. G. Economou, *J. Phys. Chem. C* **2016**, *120*, 8116.
[14] M. Al-Ghoul, R. Issa, M. Hmadeh, *CrystEngComm* **2017**, *19*, 608.
[15] D. Saliba, M. Ammar, M. Rammal, M. Al-Ghoul, M. Hmadeh, *J. Am. Chem. Soc.* **2018**, *140*, 1812.

[16] B. A. Grzybowski, *Chemistry in Motion: Reaction-Diffusion Systems for Micro-and Nanotechnology*, John Wiley & Sons, Chichester, UK **2009**.
[17] M. Al-Ghoul, M. Ammar, *Defect Diffus. Forum* **2011**, *312–315*, 800.
[18] a) G. A. Al Akhrass, M. Ammar, H. El-Rassy, M. Al-Ghoul, *RSC Adv.* **2016**, *6*, 3433; b) R. M. Walliser, F. Boudoire, E. Orosz, R. Tóth, A. Braun, E. C. Constable, Z. Rácz, I. Lagzi, *Langmuir* **2015**, *31*, 1828.
[19] M. Al-Ghoul, M. Ammar, R. O. Al-Kaysi, *J. Phys. Chem. A* **2012**, *116*, 4427.
[20] a) I. Lagzi, D. Ueyama, *Chem. Phys. Lett.* **2009**, *468*, 188; b) H. K. Henisch, *Crystals in Gels and Liesegang Rings*, Cambridge University Press, Cambridge **2005**; c) M. Al-Ghoul, R. Sultan, *J. Phys. Chem. A* **2003**, *107*, 1095; d) M. Al-Ghoul, R. Sultan, *J. Phys. Chem. A* **2001**, *105*, 8053; e) E. Ramírez-Álvarez, F. Montoya, T. Buhse, W. Rios-Herrera, J. Torres-Guzmán, M. Rivera, G. Martínez-Mekler, M. F. Müller, *Sci. Rep.* **2016**, *6*, 23402.
[21] K. Jablczynski, *Bull. Soc. Chim. Fr.* **1923**, *33*, 1592.
[22] T. Antal, M. Droz, J. Magnin, Z. Rácz, M. Zrinyi, *J. Chem. Phys.* **1998**, *109*, 9479.
[23] M. Droz, J. Magnin, M. Zrinyi, *J. Chem. Phys.* **1999**, *110*, 9618.
[24] S. Sadek, R. Sultan, in *Precipitation Patterns in Reaction–Diffusion Systems* (Ed: I. Lagzi), Research Signpost, Kerala, India **2010**.
[25] E. Nakouzi, O. Steinbock, *Sci. Adv.* **2016**, *2*, e1601144.
[26] K. M. Choi, H. J. Jeon, J. K. Kang, O. M. Yaghi, *J. Am. Chem. Soc.* **2011**, *133*, 11920.
[27] J. Rahbani, A. R. Behzad, N. M. Khashab, M. Al-Ghoul, *Electrophoresis* **2013**, *34*, 405.
[28] J. Zhang, Z. Lin, Y. Lan, G. Ren, D. Chen, F. Huang, M. Hong, *J. Am. Chem. Soc.* **2006**, *128*, 12981.
[29] J. Zhang, T. Zhang, D. Yu, K. Xiao, Y. Hong, *CrystEngComm* **2015**, *17*, 8212.